

# Continuous-flow thermal gradient PCR

Niel Crews · Carl Wittwer · Bruce Gale

© Springer Science + Business Media, LLC 2007

**Abstract** Continuous-flow thermal gradient PCR is a new DNA amplification technique that is characterized by periodic temperature ramping with no cyclic hold times. The device reported in this article represents the first demonstration of hold-less thermocycling within continuous-flow PCR microfluidics. This is also the first design in which continuous-flow PCR is performed within a single steady-state temperature zone. This allows for straightforward miniaturization of the channel footprint, shown in this device which has a cycle length of just 2.1 cm. With a linear thermal gradient established across the glass device, the heating and cooling ramp rates are dictated by the fluid velocity relative to the temperature gradient. Local channel orientation and cross-sectional area regulate this velocity. Thus, rapid thermocycling occurs while the PCR chip is maintained at steady state temperatures and flow rates. Glass PCR chips ( $25 \times 75 \times 2$  mm) of both 30 and 40 serpentine cycles have been fabricated, and were used to amplify a variety of targets, including a 181-bp segment of a viral phage DNA ( $\Phi$ X174) and a 108-bp segment of the Y-chromosome, amplified from human genomic DNA. With this unique combination of hold-less cycling and gradient temperature ramping, a 40-cycle PCR requires less than 9 min, with the resulting amplicon having high yield and specificity.

**Keywords** PCR · Rapid cycling · Continuous-flow · Thermal gradient · Microfluidics

## 1 Introduction

Continuous-flow polymerase chain reaction (CF-PCR) is an amplification technique in which a single fluidic channel is heated with spatial temperature variations such that a flowing sample experiences the thermal cycling required to induce amplification. This heating method reduces the thermal load to only that of the sample being amplified. By excluding the substrate from the thermal cycling, lower energy consumption and faster cycling can be achieved. This has been demonstrated with a variety of thermocycling techniques, including infrared (IR) heated PCR systems (Roper et al. 2007), shuttle PCR devices (Chiou et al. 2001), and CF-PCR instrumentation. CF-PCR was first demonstrated in a microfluidic device by Kopp and coworkers (Kopp et al. 1998). This foundational design consisted of a microfluidic serpentine channel embedded within a glass substrate. Three heaters were fixed to the chip to produce distinct thermal zones through which the fluid would pass. Other researchers have continued to improve the operation of this original 20-cycle device. Li and coworkers (Li et al. 2006) built a device whose 20-cycle serpentine microchannel was narrower in the regions between the three temperature zones, thus reducing the inter-temperature transition time. Schneegass and coworkers (Schneegass et al. 2001) built a 25-cycle device from silicon and glass. The device included integrated heaters and temperature sensors which were fabricated on-chip using IC manufacturing technology. Fukuba and coworkers (Fukuba et al. 2004) were able to automate the operation of a 30-cycle device using miniature pumps and valves. Sun and coworkers (Sun et al. 2002) have developed a 30-cycle CF-PCR device with integrated ITO heaters (indium tin oxide), thus making the device optically transparent. Obeid and coworkers (Obeid et al. 2003b) presented a device capable of the reverse transcription of RNA prior to its amplification in a 40-cycle serpentine channel (RT-PCR). The device was

---

N. Crews · B. Gale (✉)  
Department of Mechanical Engineering, University of Utah,  
Salt Lake City, UT 84112, USA  
e-mail: bruce.gale@utah.edu

C. Wittwer  
Department of Pathology, University of Utah,  
Salt Lake City, UT 84112, USA

fabricated with outlets at cycle numbers 20, 25, 30, 35, and the full 40. In addition, the researchers were able demonstrate amplification with plug flow, thus reducing the amplification volume to only 2  $\mu\text{l}$  per amplified sample. While these previous projects do represent significant improvements for CF-PCR, they all implement the original heating scheme: multiple zones of distinct temperatures, placed in parallel, through which a serpentine channel repeatedly passes. An alternative layout was presented by Hashimoto and coworkers (Hashimoto et al. 2004), who developed a device in which the isothermal zones were separated into the four quadrants of a rectangular substrate. By fabricating a 20-loop spiral microchannel which passes repeatedly through each zone, the flowing fluid was able to experience the required thermocycling.

Integration of these continuous-flow amplification systems is currently being accomplished by several groups. Obeid and coworkers (Obeid and Christopoulos 2003a) have combined a continuous-flow RT-PCR with a laser-induced fluorescence (LIF) detection system. Nakayama and coworkers (Nakayama et al. 2006) have demonstrated real-time amplification detection using TaqMan technology. Wang and coworkers (Wang et al. 2006) have used a quadrant heating/spiral channel CF-PCR device as an amplification module within a Sanger sequencing system. In addition, other technologies are being developed that could potentially be included to form a complete “Lab-on-a-chip”, such as continuous-flow DNA extraction (Cao et al. 2006) and sample mixing (Garstecki et al. 2006).

The further miniaturization and simplification of the CF-PCR device is critical for this technology to compete against other micro-PCR methods. Researchers have shown that by including insulating features in the fabricated devices, better thermal separation between the several temperature zones is possible (Hashimoto et al. 2004; Schneegass et al. 2001; Yang et al. 2005). While this allows for a reduction in the spacing between the heaters, thermal “cross-talk” ultimately limits the proximity of the isothermal regions (Li et al. 2006). Thus, the need for multiple isolated temperature zones greatly complicates further reduction in the CF-PCR footprint.

This challenge has been circumvented by the development of the current device, which uses a steady-state temperature gradient to create the desired fluidic thermocycling protocol within a single thermal zone. Whereas the multi-zone systems require distance and insulation to maintain the isothermal regions, the distribution of isothermal lines within the single-zone gradient system occurs spontaneously and can be easily adjusted by changing the heat flux through the substrate. In this way, the spatial distribution of the required PCR temperatures can be significantly reduced, resulting in a much smaller channel footprint, with no increase in device complexity. Additionally, by reducing two-dimensional (2D) isothermal *areas* into one-

dimensional (1D) isothermal *lines*, residence times can be eliminated. Extensive research on the reaction kinetics of PCR has shown that residence times are not required to denature or anneal, as long as sample equilibrium is achieved. (Wittwer and Hermann 1999) Conventional PCR instrumentation has been used to demonstrate that hold-less cycling protocols can reduce amplification time, create no loss in amplification efficiency, and result in superior amplification specificity (Wittwer and Hermann 1999). In the thermal gradient system, ramp rates are the designed characteristic. Local ramp rates are dictated by the fluid velocity relative to the isothermal lines. The local velocity is determined by channel orientation and cross-sectional area. It is known that polymerase activity is the dominant rate limiting factor in PCR, with typical extension rates that can approach 100 bases per second. Thus, for short DNA targets (<200 bp) the ideal cycling protocol consists of temperature spikes to denature then anneal, followed by a moderate thermal ramp through the extension temperature. This has now been achieved with the design of the thermal gradient PCR system.

## 2 Experimental

### 2.1 Heater assembly

To generate the desired temperature gradient across the device, a platform was built to uniformly heat a  $75 \times 25$  mm PCR chip along one long edge and cool along the opposite edge, inducing a steady-state temperature gradient in the glass. By controlling the amount of heat applied to the hotter edge of the chip and the heat withdrawn from the cooler edge, the thermal gradient can be adjusted. The glass device rests on two aluminum strips, 6.35 mm wide, which extend the length of the chip. The strip corresponding to the cooler edge is coupled to a network of cooling fins. Thin-film heaters (HR5200, Minco, MN, USA) are fixed beneath both strips—beneath the hot strip to introduce heat into the PCR chip, and beneath the cool strip to allow for the regulation of heat transfer from the chip to the cooling fins. To secure and insulate the apparatus, the components of the assembly have been fixed to a machined Teflon base. Fig. 1 shows a diagram of the designed heater assembly.

### 2.2 Chip design

“Rapid” thermal cycling has been defined as a protocol with cycle times less than 60 s (Wittwer et al. 1994). This thermal gradient PCR device has been designed to operate significantly faster than this designated limit. The desired thermocycling protocol begins with the PCR sample being brought to the denaturing temperature for several seconds,

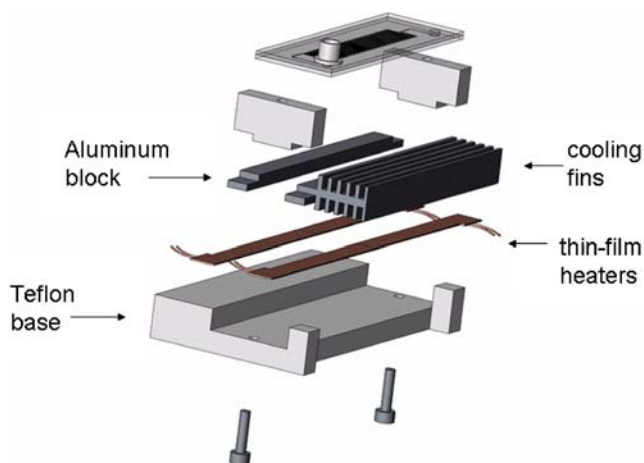


**Fig. 1** An exploded diagram of the heating apparatus designed for use with thermal gradient PCR. Aluminum pieces thermally interface the glass chip with the heaters and cooling fins, ensuring a uniform temperature gradient across the glass. The Teflon pieces hold the heating elements in place

to ensure that the template DNA is fully denatured. The sample is then cooled to the annealing temperature at a rate greater than  $10^{\circ}\text{C}/\text{s}$ , after which the sample temperature immediately begins to increase steadily toward the denaturing temperature at a rate between 1 and  $4^{\circ}\text{C}/\text{s}$ . At the moment when the sample reaches the denaturing temperature, it is again rapidly cooled. This “quick cool/slow heat” ramping protocol continues for at least 30 cycles, during which the desired DNA target amplifies to an appropriately high concentration. Although slow heating is only needed up to the extension temperature, for simplicity the current design heats at a constant rate.

A “hold-less” cycling protocol with varying temperature ramp rates can be achieved by establishing a thermal gradient within the glass chip such that the parallel isothermal lines run the length of the device. A serpentine microfluidic channel is imbedded in the glass. At locations along the channel where the sample should be held at a specific temperature, the channel section is located along the appropriate isothermal line. Where temperature ramping is desired, the channel passes perpendicularly across the isothermal lines. Where rapid temperature change is desired, the channels are as narrow as the fabrication process will allow, so that the sample flows quickly across the isothermal lines. Conversely, in the regions designated for slow heating, the channels are wider, which creates a slower sample velocity and thus a slower rate of temperature change. The geometry of a representative mask is shown in Fig. 2. The 30-cycle and 40-cycle chips are fabricated from  $75 \times 25$  mm glass blanks. The design depth for the 30-cycle chip is a uniform  $50 \mu\text{m}$ . The channel widths are 110 and  $650 \mu\text{m}$ , for the cooling and heating regions, respectively, with the passes of the channel spaced  $450 \mu\text{m}$  apart. The 40-cycle chip has a channel depth of

$40 \mu\text{m}$  and channel widths of 110 and  $440 \mu\text{m}$ , with a spacing of  $400 \mu\text{m}$  between the channel passes. By these design parameters, the ratio between the average cooling and heating rates is approximately 6:1 for the 30-cycle chip and 4:1 for the 40-cycle chip.

### 2.3 Chip fabrication

The PCR chips are fabricated from soda lime glass microscope slides (12-550A, Fisher Scientific, NH, USA) that were pre-cleaned with a piranha etch ( $3 \text{H}_2\text{SO}_4/1 \text{H}_2\text{O}_2$ ) for 10 min. A  $900 \text{ nm}$  thick film of chromium was then sputtered onto the glass blanks. Following the chromium deposition, a  $2 \mu\text{m}$  thick layer of photoresist (Shipley, 1813) was spun onto the slides. The photoresist was then patterned using standard mask lithographic procedures, followed by a hard bake at  $120^{\circ}\text{C}$  for 1 h. The glass was then dipped into a chromium etchant to remove the exposed metal. With the cured photoresist and the thin chromium film serving as an etch mask for the top side of the glass, the backside of the glass was protected from the glass etchant with DuPont Kapton tape. The glass slides were then immersed in an etchant bath ( $1 \text{HF}/3 \text{HNO}_3/10 \text{H}_2\text{O}$ ) until the desired etch depth was achieved (etch rate  $\sim 1.5 \mu\text{m}/\text{min}$ ). After stripping off the remaining photoresist and chromium, inlet and outlet holes were drilled through the patterned glass using a diamond-tipped drill bit and drill press. The glass slides were again cleaned in a piranha etch, along with an equal number of blank slides. Each patterned and drilled slide was then fused to a blank slide by baking at  $620^{\circ}\text{C}$  for 4 h, using a protocol similar to that given by

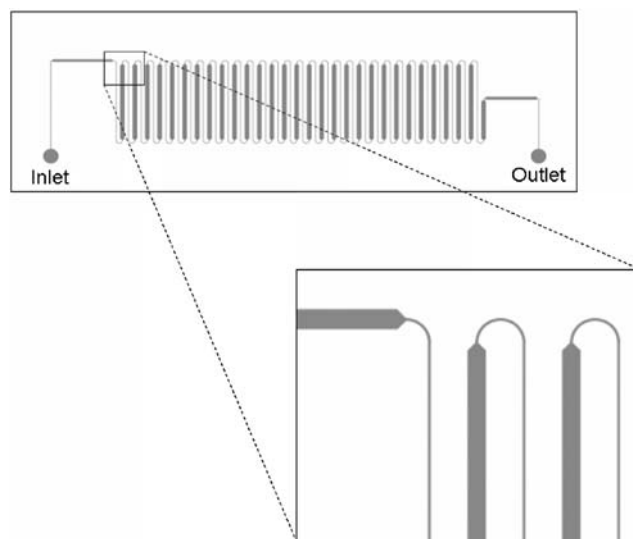


**Fig. 2** The mask geometry for the 30-cycle PCR chip shows the layout of the serpentine channel. The channel is etched into  $25 \times 75$  mm glass pieces. The mask dimensions for the wide and narrow regions are  $550$  and  $10 \mu\text{m}$ , respectively. Considering the isotropic nature of the etchant, the final widths of the channel are  $650$  and  $110 \mu\text{m}$ , respectively

Simpson and coworkers (Simpson et al. 1998). Upon cooling, a Nanoport fluidic interconnect (Upchurch Scientific, WA, USA) was attached over the inlet hole of each chip.

#### 2.4 Temperature measurement

The fabricated PCR chips were affixed to the heating assembly with a small amount of thermal grease. Kapton tape was used to attach two thermocouples (Omega, CT, USA) to the top surface directly above the serpentine channel, at the location of the hottest and coolest temperatures. To examine the uniformity of the temperature gradient across the entire chip, an infrared camera (Thermacam PM390, Inframetrics Inc., MA, USA) was used to capture thermal images of the device. To remove uncertainties associated with the emissivity of the glass, chips used for the thermal imaging calibration were spray painted black (Krylon, Sherwin-Williams, OH, USA). A DC voltage was then applied to the heaters, and approximately 10 min was allowed for the system to equilibrate. Once the thermal gradient stabilized, measurements from the thermocouples and the IR camera were recorded and compared. Once the temperature of the chip surface was known, the temperature of the microchannel ( $T_c$ ) within the glass was obtained from the following equation:

$$T_c = \left( \frac{Lh}{k} + 1 \right) \cdot (T_s - T_\infty) + T_\infty \quad (1)$$

where  $L$  is the distance from the chip surface to the imbedded channel,  $h$  is the average convective heat transfer coefficient at the surface/air interface,  $k$  is the thermal conductivity of the glass,  $T_s$  is the temperature of the surface, and  $T_\infty$  is the ambient temperature.

There is also a lateral temperature distribution within the microchannel due to heat transfer through the flowing fluid. With a linear temperature gradient across the substrate, a constant heat rate exists in the channel sections that run in the direction of the gradient. The fully developed temperature profile under this condition can be found analytically for basic channel geometries (Kays and Crawford 1993). For a circular channel, the lateral temperature distribution ( $T$ ) is given as:

$$T = T_c - \frac{2V}{\alpha} \frac{dT_m}{dx} \left( \frac{3r_0^2}{16} + \frac{r^4}{16r_0^2} - \frac{r^2}{4} \right) \quad (2)$$

where  $T_c$  is the temperature at the channel wall,  $V$  is the average fluid velocity,  $\alpha$  is the molecular thermal diffusivity,  $dT_m/dx$  is the temperature gradient along the channel wall (in the direction of fluid flow),  $r_0$  is the radius of the channel, and  $r$  is the distance from the centerline at which the fluid temperature ( $T$ ) is calculated.

#### 2.5 PCR experiments

To demonstrate the capability of the thermal gradient PCR chip, small targets were amplified from both viral DNA and human genomic DNA. As part of these tests, a 110-bp and 181-bp segment of a viral phage DNA template ( $\Phi$ X174,  $10^5$  copies/ $\mu$ l) were amplified on a 30-cycle chip, and a 108-bp segment of the Y-chromosome was amplified from human genomic DNA (5 ng/ $\mu$ l) on the 40-cycle chip. In addition to the template DNA, the PCR mixture used for amplification consisted of 0.5  $\mu$ M of each primer<sup>1</sup>, 200 mM of each deoxynucleotide triphosphate (dNTP), 0.4 U of KlenTaq1 polymerase (AB Peptides, MO, USA), 88 ng of TaqStart antibody (ClonTech, CA, USA), 3 mM MgCl<sub>2</sub>, and 1X LCGreen Plus (Idaho Technology, UT, USA) in 50 mM Tris (pH 8.3) and 250 ng/ml bovine serum albumin (BSA). To compare amplification characteristics (speed, specificity, and yield), portions of each PCR mixture were amplified in both the thermal gradient PCR chip and commercial PCR equipment (LightCycler®, Roche, IN, USA). To validate the amplification, negative controls (without template DNA) were also amplified to ascertain whether the resulting amplicon is a product of residual contamination.

Since the chips were to be used for a substantial number of amplification experiments, a cleaning protocol was developed to effectively remove the residual DNA from the microchannel. The protocol consists of a 100  $\mu$ l purification wash of 15% Clorox bleach and 2% detergent (7X-O-Matic, ICN Biomedicals, OH, USA), followed by two 100  $\mu$ l plugs of deionized water separated by a 50  $\mu$ l plug of mineral oil. The cleaning/rinsing reagents were passed through the chip at a flow rate of approximately 30  $\mu$ l/min. With the PCR chip in the heating assembly and the thermal gradient established, PCR was performed by loading the PCR mixture into a syringe (1705, Hamilton, NV, USA) and pumped (KDS120, KD Scientific, MA, USA) continuously through the chip at a steady rate. The PCR sample containing the viral template was pumped through the 30-cycle chip at a rate of 1.5  $\mu$ l/min. The sample containing the human genomic template was pumped through the 40-cycle device at a rate of 2  $\mu$ l/min. After filling the channel, sample began to collect at the outlet hole, from which it was collected in 5  $\mu$ l increments for analysis. After the desired amount of sample was passed through the channel, the system was cleaned as explained. Serial experiments were performed to determine any cross-

<sup>1</sup> The primer sequences for the selected targets are as follows:  $\Phi$ X174, 110-bp (F - GGTTCTCAAGGACTGGTTT, R - TTGAACAGC ATCGGACTCAG)  $\Phi$ X174, 181-bp (F - GCTTCCATGACGCA GAAGTT, R - GCGAAAGGTCGCAAAGTAAG) Y-chromosome, 108-bp (F - ATTACACTACATTCCCTTCCA, R - AGTGAAATTGT ATGCAGTAGA)

contamination between samples. For serial experiments, the thermal gradient was left unchanged while the pumping, removal, and cleaning protocols were repeated for each successive sample. Positive and negative controls from both the thermal gradient PCR chip and the LightCycler were analyzed on a stained 1.5% agarose gel.

### 3 Results and discussion

Figure 3 shows photographs of the completed device, which measures approximately  $8 \times 10 \times 2$  cm. External interfaces to the system include the electrical leads for the thin-film heaters and the Nanoport fitting (in the figure, bottom left corner of the chip) where the PCR samples are introduced. During fabrication of the glass channel, etched features were measured with a stylus profilometer (P-10, KLA-Tencor, CA, USA). Dimensions were found to be within 5% of the design specifications. As assembled, the channel is not directly above the aluminum strips. Rather, it is located between the strips, where the temperature gradient is linear and where the entire channel is optically accessible from above and below.

#### 3.1 Temperature calibration

Equation 1 was used to approximate the channel temperature from the measured surface temperature. The approximate distance between the glass surface and the microchannel ( $L$ ) is 0.95 mm; the thermal conductivity ( $k$ ) of borosilicate glass is 1.1 W/m-K; the average heat transfer coefficient ( $h$ ) is approximately 5 W/m<sup>2</sup>-K for the temperatures to which the device will be subject. Using these values and an ambient temperature of 22°C, the difference between the surface temperature and the channel temperature is less than 0.4°C.

The approximate lateral temperature distribution within the microchannel has been calculated using Eq. 2. Assuming a molecular thermal diffusivity of  $164 \times 10^{-9}$  m<sup>2</sup>/s (water at 80°C), a hydraulic diameter of 100 μm, an average fluid velocity of 10 mm/s, and an axial temperature gradient of 4 deg/mm, the lateral variation in temperature within the channel will be on the order of 0.25°C. This temperature lag, making the fluid in the center of the channel cooler during heating and warmer during cooling, can be considered to have a negligible effect on the PCR efficiency.

With the device fully assembled, voltage was applied to the heaters. After 10 min, equilibrium was established such that the microfluidic channel was within a stable temperature distribution bounded by 95 and 60°C ( $\pm 1^\circ\text{C}$ ). The surface temperature was measured at two locations with the thermocouples, and then the entire surface was imaged with the infrared camera. Figure 4 shows a typical image

recorded by the IR camera, as well as a pseudo-3D image of the same data, which allows for better visualization of the temperature gradient across the chip. The glass in the region of the microfluidic channel experiences an average temperature gradient of 3.5°C/mm, as shown in Fig. 5. Above approximately 78°C the gradient is higher than the average, reaching a maximum value of 4.5°C/mm at the denaturing temperature. Below 78°C the gradient slightly decreases, with a 2.5°C/mm minimum at the annealing temperature.

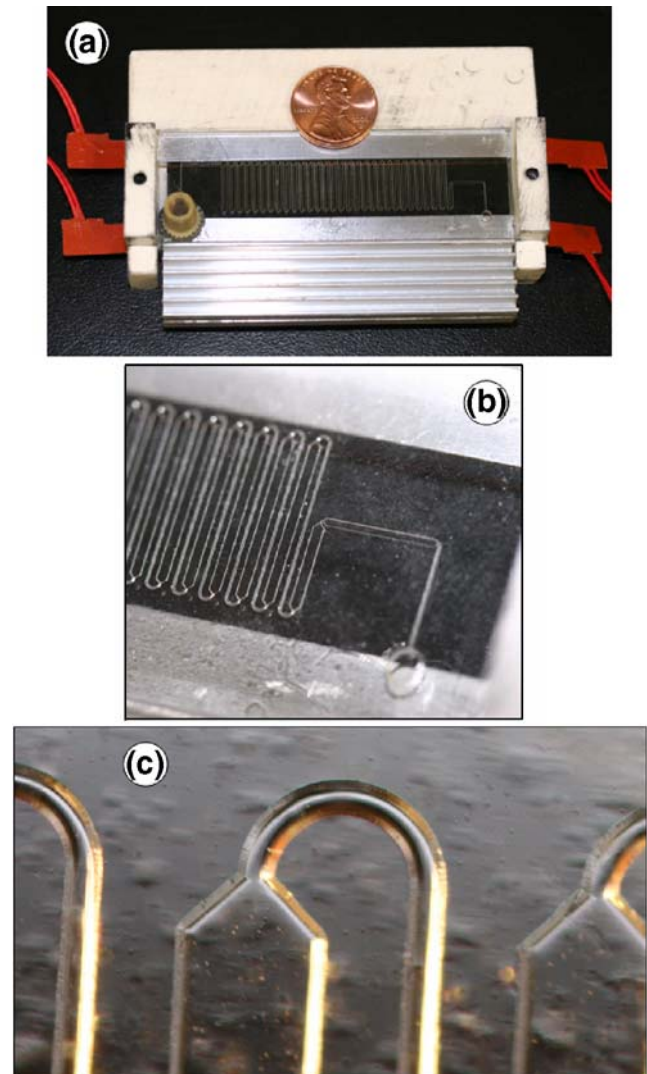


**Fig. 3** (a) The microfabricated glass chip rests on the two aluminum strips of the heating assembly. Electrical connections to the thin-film heaters beneath both strips are visible. A thermal gradient is induced across the glass by heating one strip (beneath the top edge of the chip, in the image) and drawing heat from the other strip by means of cooling fins. As the PCR mixture travels through the device (from left to right, in the image), it is heated and cooled repeatedly (30× in this particular device). (b) The serpentine channel within the chip is located in the region between the strips, where the temperature gradient is virtually linear. The channel is narrow where rapid temperature change is desired and wide where slow ramp rates are needed. (c) The etching of the glass produces smooth, curved channel sidewalls

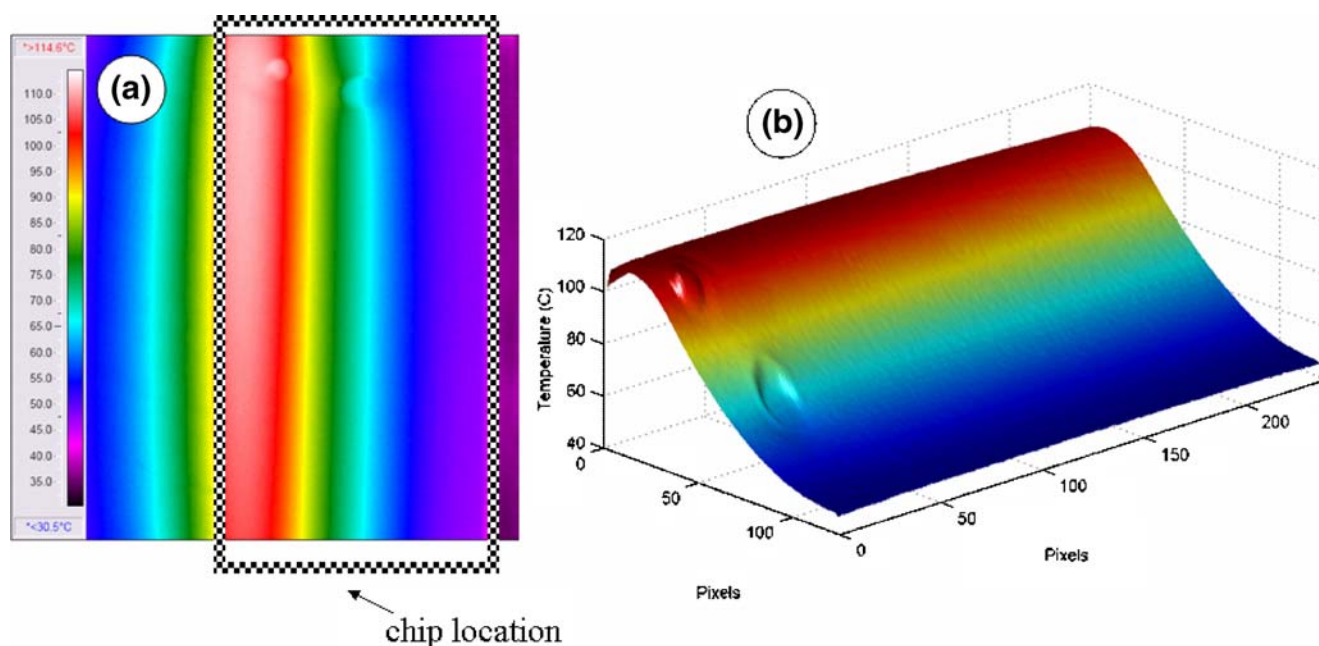


**Fig. 4** With the thermal gradient device painted black, the temperature was measured with an IR camera. (a) The IR camera generates a 2D color image displaying temperature. (b) Graphing the IR data in a pseudo-3D format allows for visual characterization of the thermal gradient

The curvature of the gradient results from the convection of heat away from the surface of the glass. Were the chip completely insulated the heat transfer would be strictly one-dimensional and the temperature distribution would be perfectly linear. However, this variation in the gradient is a favorable one for PCR, since the critical ramping time is between the annealing and extension temperatures. Therefore, insulating the surface is unnecessary.

### 3.2 Stochastic variation in individual DNA velocities

Under proper amplification conditions, there are only two sizes of DNA in the microfluidic channel: the template DNA of very large size (kbp, Mbp, or more), and the amplicon, which commonly does not exceed 200 bp in length. The 1-dimensional molecular diffusion coefficient for the shorter strands is on the order of  $200 \mu\text{m}^2/\text{s}$  (Lapham et al. 1997; Pappaert et al. 2005). This mobility corresponds to random Brownian displacement on the order of  $25 \mu\text{m}$  every 1.5 s. With a channel depth of  $50 \mu\text{m}$  and an average heating time of 15 s, it is likely that each DNA molecule spends significant time in all velocity streamlines. Thus, the average value of the fluid velocity can likewise be assumed for all small DNA fragments. For very large DNA (>100 kbp), hydrodynamic effects dominate, and the DNA is drawn into the faster flow regions toward the center of the channel, being found to always migrate with a size-dependent velocity between the average and the maximum fluid velocity (Jendreck et al. 2003). For these reasons, variations in individual velocities for both the template DNA and the generated amplicon can be ignored, and

average values can be assumed. While self-diffusion rates for the other PCR constituents may vary, individual dwell times for these molecules are irrelevant.

### 3.3 PCR results

The control samples were amplified on the LightCycler in 10 min for the 30-cycle PCR and 13 min for the 40-cycle PCR. By pumping sample through the 30-cycle thermal gradient chip at  $1.5 \mu\text{l}/\text{min}$ , sample started to accumulate at

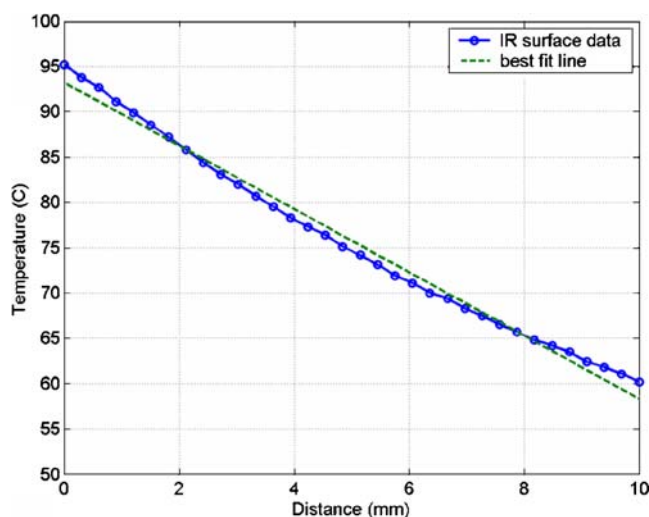


**Fig. 5** The temperature gradient of the glass surface above the microfluidic channel is nearly linear at  $3.5^\circ\text{C}/\text{mm}$  ( $\pm 1^\circ\text{C}/\text{mm}$ ). Since the activity of the DNA polymerase enzyme limits the allowable ramp rates between the annealing and extension temperatures, the shallower gradient at lower temperatures is advantageous

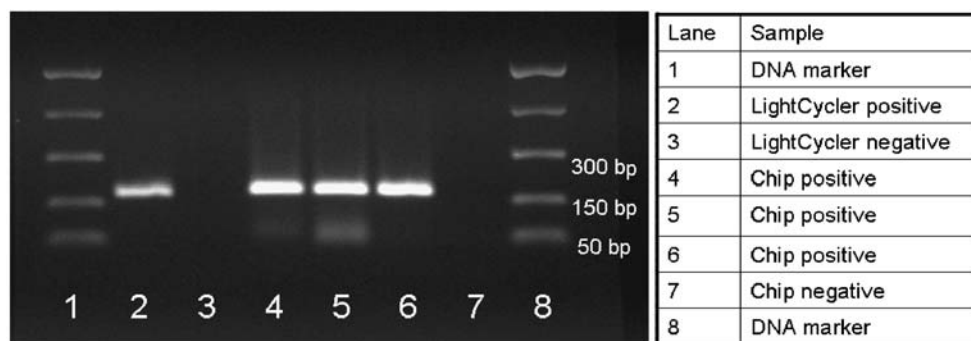


**Fig. 6** Fluorescent image of PCR products separated in a 1.5% agarose gel after a 30-cycle amplification. The target is a 181-bp segment of the  $\Phi$ X174 phage DNA. Samples from the LightCycler were amplified in 10 minutes and positive and negative controls are shown in lanes 2 and 3, respectively. Lanes 4–8 show consecutive

samples amplified in the thermal gradient PCR chip (11 min per sample), the last of which was a negative control. The slightly brighter signal from the chip-amplified product is due to partial evaporation of the sample. Faint bands associated with primer dimers are visible

the outlet hole after 11 min, averaging 22 s per amplification cycle. Within each cycle, the sample was cooled from 95 to 60°C in approximately 3 s or an average cooling rate of nearly 12°C/s. The heating occurred over 18 s, at a rate of approximately 2°C/s. For the 40-cycle PCR chip pumped at 2  $\mu$ l/min, the sample began to exit after 8.5 min, 35% faster than the LightCycler. The average cycle time for this PCR was less than 13 s, with average cooling and heating rates of 14 and 3°C/s, respectively. Both chip designs were used for multiple amplifications by repeating the pump/remove/clean protocol, after which representative sample volumes were analyzed on electrophoresis gels. Consecutive amplifications of identical PCR samples, as shown in Fig. 6, indicate the repeatability of the thermal gradient device. By amplifying different targets in serial fashion, as shown in Fig. 7, the absence of cross-contamination between samples is demonstrated. Amplifying negative samples before and after a positive sample, as shown in Fig. 8, confirms that the amplicon was copied from the intended template. The cleaning protocol was able to

adequately remove the PCR residue between amplifications, allowing for extended use with biological samples.

A precise way to determine the efficiency of a PCR device is to compare the real-time amplification of serially diluted template of known concentration. The thermal gradient PCR chip is not currently compatible with real-time detection. Estimates of efficiency and specificity were therefore made by visual comparison of gel electrophoregrams of sample amplified on the microchip and the control system. Since the chip-amplified product is generally as concentrated and as clean as that of the LightCycler, comparable amplification efficiency and specificity can be assumed.

When the 40-cycle thermal gradient chip was cycled 35% faster than the LightCycler, lower yield was consistently obtained. Lower yields with faster cycle times are a common finding in the CF-PCR literature (Hashimoto et al. 2004; Kopp et al. 1998; Schneegass et al. 2001). While no attempt was made to amplify DNA targets above 200 bp in length, it should be noted that the great majority of genetic testing and pathogen detection involve target sequences less than 200-bp

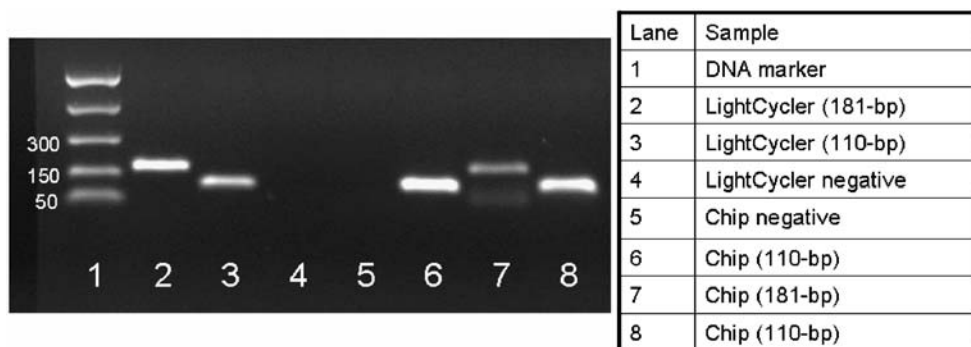


**Fig. 7** Samples amplified in this experiment include positive and negative samples of 110-bp and 181-bp, amplified from  $\Phi$ X174 phage DNA. Samples from both the LightCycler (30 cycles in 10 min) and the thermal gradient PCR chip (30 cycles in 11 min) are shown. The sample

order for the chip amplification (negative, 110-bp, 181-bp, 110-bp) was used to confirm the lack of cross-contamination between samples. Faint bands associated with primer dimers are visible

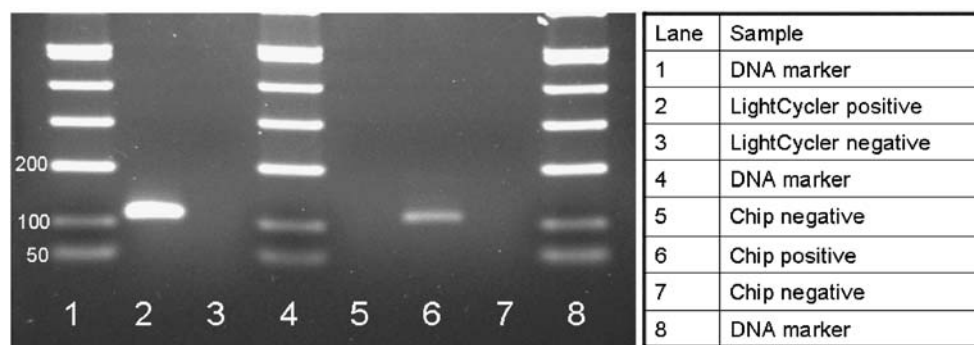


**Fig. 8** Samples containing primer sets corresponding to the 108-bp product were amplified from human genomic DNA with a 40-cycle PCR. Samples amplified on the LightCycler (13 min) and on the thermal

gradient PCR chip (8.5 min) are shown. The negative controls (*lanes 5, 7*) passed through the device before and after the positive amplification (*lane 6*) to confirm that the amplification is from genomic template

in size. For this reason, the initial testing of the device focused on the lower range of target sizes. While it is probable that the gradient system will have a low limit on the size of amplifiable target, such applications are not common enough to be considered a noteworthy disadvantage of the system.

### 3.4 Microchip PCR

While high through-put is the desired characteristic for applications such as drug discovery, and genetic scanning/mapping, it is fast turn-around time for single- or several-sample analyses that will allow for the development of integrated palm-top or bench-top medical instruments. When trained professionals are provided such tools for rapid pathogen-detection or disease genotyping, the accuracy and timeliness of medical diagnosis and treatment will improve.

A single experiment can be performed in approximately 1 h. In addition to the amplification time, this includes 10 min for the instrument to warm up, 5 min to prepare the PCR sample from pre-extracted DNA and other prepared reagents, 5 min for sample loading, 5 min for the extraction of each of the several 5  $\mu$ l aliquots, and 15 min to clean the chip between samples and allow for the temperature gradient to re-stabilize. The overall time of experiment can potentially be halved by reducing the number of aliquots collected, and preparing multiple samples in advance. Although the thermal gradient PCR device operates with a reduced amplification time, all other periphery processes (DNA extraction, sample mixing, post-processing) follow traditional laboratory-based protocols. Thus, the total time of experiment is not significantly reduced. Significant, competitive reduction in overall time will only come through full integration of all preparatory and analytical steps (Easley et al. 2006).

Two primary metrics for micro-PCR are the speed of the amplification and the size of the device. Figure 9 graphs these two characteristics for the current design as well as for previous CF-PCR devices. While some previous CF-

PCR devices have been operated with similarly rapid cycle times, and some have approached the small footprint of the thermal gradient device, only through this present technique have both high speed and small size been achieved together. This can be attributed to the single-zone temperature profile of the device, allowing for short cycle length with no residence times, and the reasonably high width ratios that produce the required slow heating rate with fast cooling. It can be concluded that further reduction of both the device footprint and cycle time can be obtained by making intuitive adjustments in the thermal gradient profile and channel geometry.

A single drop of blood contains on the order of  $10^6$  copies of genomic DNA, which could theoretically be used at a strong concentration (1,500 copies/ $\mu$ l) for multiple

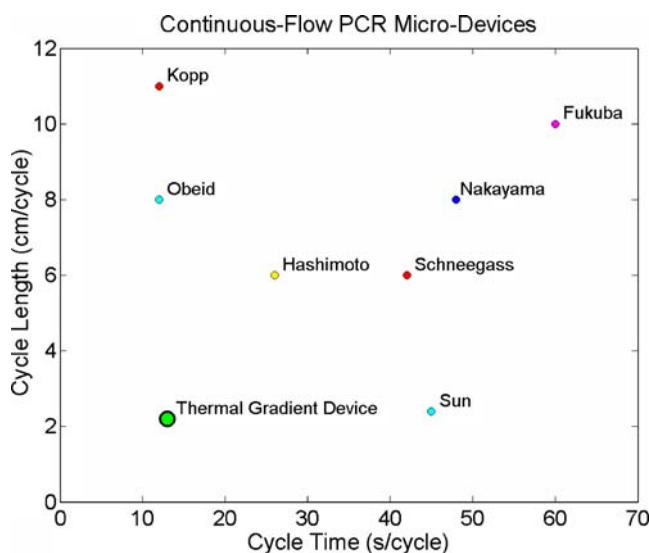


**Fig. 9** Graphical summary of the several CF-PCR designs, indicating the reported cycle time and cycle length for each device. Shorter cycle time implies faster amplification, and shorter cycle length results in a smaller device footprint. Previous designs are labeled with the corresponding first author. The device presented in this article is labeled “Thermal Gradient Device”

PCR reactions. Thus, the lower concentration limits would not be of concern for human genetic diagnostics. However, for viral or bacterial detection, small samples would yield template concentration much lower, requiring a higher level of sensitivity. The required sensitivity of this thermal gradient PCR device has not been explored.

Were the amplicon able to be both detected and quantified on-chip, the total time of experiment would be significantly reduced. By detecting product amplification (Nakayama et al. 2006), initial template concentration can be determined. For further characterization of the amplicon (sequencing, mutation detection, sizing, etc.), additional off-chip analysis is normally required. However, the unique spatial spreading of the different PCR stages in this thermal gradient device introduces the opportunity for identifying the amplified product during the PCR, thus totally eliminating the need for additional time or sample transport for successive testing. Since each location along the channel possesses a unique cycle/temperature identity, fluorescence imaging techniques could be used to characterize both the amplification behavior and the unique dsDNA melting signature of the amplicon (Ririe et al. 1997) from a single fluorescence image of the device (Mao et al. 2002). Such an approach would also eliminate the oft-cited disadvantage of cycle number flexibility commonly associated with CF-PCR systems (Obeid et al. 2003b), since the product analysis could theoretically be performed for all cycles at once. This proposed integration with fluorescence analysis is possible with precise mapping of the temperature distribution and the clear optical access to the entire channel that is achieved with thermal gradient PCR.

#### 4 Conclusion

This new continuous-flow thermal gradient PCR technique is capable of rapidly amplifying DNA targets from both viral and human genomic DNA. A microfluidic thermocycling protocol was instituted with no hold times and ramp rates based on reaction kinetics. This was achieved by inducing a quasi-linear temperature gradient in a glass microfluidic chip containing a uniquely designed serpentine channel. Cycle times of 13 s are sufficient to amplify targets from human genomic DNA. A cleaning protocol was developed to allow serial amplification of different PCR samples on the same chip without cross-contamination between the samples. Anticipated further advancements in the system include the on-chip integration with pre-amplification processes such as DNA extraction and sample mixing, and post-amplification analyses for amplicon detection, quantification, and characterization.

**Acknowledgement** Authors acknowledge the Utah State Center of Excellence Grants, the University of Utah Synergy Program, and the NSF IGERT Program for the funding of this work. Authors also wish to thank the respective members of the Wittwer and Gale research labs, whose valued contributions have allowed for this project to advance at a welcome pace.

#### References

- W. Cao, C.J. Easley, J.P. Ferrance, J.P. Landers, *Anal. Chem.* **78**, 7222–7228 (2006)
- J. Chiou, P. Matsudaira, A. Sonin, D. Ehrlich, *Anal. Chem.* **73**, 2018–2021 (2001)
- C.J. Easley, J.M. Karlinsey, J.M. Bienvenue, L.A. Legendre, M.G. Roper, S.H. Feldman, M.A. Hughes, E.L. Hewlett, T.J. Merkel, J.P. Ferrance, J.P. Landers, *PNAS* **103**, 19272–19277 (2006)
- T. Fukuba, T. Yamamoto, T. Naganuma, T. Fujii, *Chem. Eng. J.* **101**, 151–156 (2004)
- P. Garstecki, M.J. Fuerstman, M.A. Fischbach, S.K. Sia, G.M. Whitesides, *Lab Chip* **6**, 207–212 (2006)
- M. Hashimoto, P.C. Chen, M.W. Mitchell, D.E. Nikitopoulos, S.A. Soper, M.C. Murphy, *Lab Chip* **4**, 638–645 (2004)
- R.M. Jendrejack, E.T. Dimalanta, D.C. Schwartz, M.D. Graham, J.J. de Pablo, *Phys. Rev. Lett.* **91**, (2003)
- W.M. Kays, M. E. Crawford. *Convective Heat and Mass Transfer* (McGraw-Hill, New York, 1993), pp. 110–116
- M.U. Kopp, A.J. de Mello, A. Manz, *Science* **280**, 1046–1048 (1998)
- J. Lapham, J.P. Rife, P.B. Moore, D.M. Crothers, *J. Biomol. Nmr.* **10**, 255–262 (1997)
- S.F. Li, D.Y. Fozdar, M.F. Ali, H. Li, D.B. Shao, D.M. Vykoukal, J. Vykoukal, P.N. Floriano, M. Olsen, J.T. McDevitt, P.R.C. Gascoyne, S.C. Chen, *Journal of Microelectromechanical Systems* **15**, 223–236 (2006)
- H.B. Mao, M.A. Holden, M. You, P.S. Cremer, *Anal. Chem.* **74**, 5071–5075 (2002)
- T. Nakayama, Y. Kurosawa, S. Furui, K. Kerman, M. Kobayashi, S.R. Rao, Y. Yonezawa, K. Nakano, A. Hino, S. Yamamura, Y. Takamura, E. Tamiya, *Anal. Bioanal. Chem.* **386**, 1327–1333 (2006)
- P.J. Obeid, T.K. Christopoulos, *Anal. Chim. Acta* **494**, 1–9 (2003a)
- P.J. Obeid, T.K. Christopoulos, H.J. Crabtree, C.J. Backhouse, *Anal. Chem.* **75**, 288–295 (2003b)
- K. Pappaert, J. Biesemans, D. Clicq, S. Vankrunkelsven, G. Desmet, *Lab Chip* **5**, 1104–1110 (2005)
- K.M. Ririe, R.P. Rasmussen, C.T. Wittwer, *Anal. Biochem.* **245**, 154–160 (1997)
- M.G. Roper, C.J. Easley, L.A. Legendre, J.A.C. Humphrey, J.P. Landers, *Anal. Chem.* **79**, 1294–1300 (2007)
- I. Schneegass, R. Brautigam, J.M. Kohler, *Lab Chip* **1**, 42–49 (2001)
- P.C. Simpson, A.T. Woolley, R.A. Mathies, *Biomed. Microdevices* **1**, 7–25 (1998)
- K. Sun, A. Yamaguchi, Y. Ishida, S. Matsuo, H. Misawa, *Sens. Actuators, B: Chem.* **84**, 283–289 (2002)
- H. Wang, J.F. Chen, L. Zhu, H. Shadpour, M.L. Hupert, S.A. Soper, *Anal. Chem.* **78**, 6223–6231 (2006)
- C.T. Wittwer, M.G. Hermann, in *PCR Applications: Protocols for Functional Genomics*, eds. by M.A. Innis, D.H. Gelfand, J.J. Sninsky (Academic, San Diego, 1999), pp. 211–229
- C.T. Wittwer, G.B. Reed, K.M. Ririe, in “*Rapid Cycle DNA Amplification.*” *The Polymerase Chain Reaction*, eds. by K.B. Mullis, F. Ferre, R. Gibbs (Springer, Deerfield Beach, 1994), pp. 174–181
- M. Yang, R. Pal, M. A. Burns, *J. Micromechanics Microengineering* **15**, 221–230 (2005)